Title
Inhibitor Bound Crystal Structures of Bacterial Nitric Oxide Synthase.

Journal
Biochemistry, 54(26)

Authors
Holden, Jeffrey
Dejam, Dillon
Lewis, Matthew
et al.

Publication Date
2015-07-07

DOI
10.1021/acs.biochem.5b00431

Peer reviewed

HHS Public Access

Author manuscript

Biochemistry. Author manuscript; available in PMC 2016 May 07.

Published in final edited form as:

Biochemistry. 2015 July 7; 54(26): 4075–4082. doi:10.1021/acs.biochem.5b00431.

Inhibitor Bound Crystal Structures of Bacterial Nitric Oxide Synthase

Jeffrey K. Holden[†], **Dillon Dejam**[†], **Matthew C. Lewis**[†], **He Huang**[‖], **Soosung Kang**[‖], **Qing Jing**[‖], **Fengtian Xue**[‖], **Richard B. Silverman**[*,‖,⊥,#], and **Thomas L. Poulos**[*,†,‡,§]

[†]Department of Molecular Biology and Biochemistry, University of California, Irvine, California 92697-3900, United States

[‡]Department of Pharmaceutical Sciences, University of California, Irvine, California 92697-3900, United States

[§]Department of Chemistry, University of California, Irvine, California 92697-3900, United States

[‖]Departments of Chemistry and Molecular Biosciences, Northwestern University, Evanston, Illinois 60208-3113, United States

[⊥]Chemistry of Life Processes Institute, Northwestern University, Evanston, Illinois 60208-3113, United States

[#]Center for Molecular Innovation and Drug Discovery, Northwestern University, Evanston, Illinois 60208-3113, United States

Abstract

Nitric oxide generated by bacterial nitric oxide synthase (NOS) increases the susceptibility of Gram-positive pathogens *Staphylococcus aureus* and *Bacillus anthracis* to oxidative stress, including antibiotic-induced oxidative stress. Not surprisingly, NOS inhibitors also improve the effectiveness of antimicrobials. Development of potent and selective bacterial NOS inhibitors is complicated by the high active site sequence and structural conservation shared with the mammalian NOS isoforms. To exploit bacterial NOS for the development of new therapeutics, recognition of alternative NOS surfaces and pharmacophores suitable for drug binding is required. Here, we report on a wide number of inhibitor-bound bacterial NOS crystal structures to identify several compounds that interact with surfaces unique to the bacterial NOS. Although binding studies indicate that these inhibitors weakly interact with the NOS active site, many of the

[*]**Corresponding Authors:** (R.B.S.) agman@chem.northwestern.edu; Phone: (847) 491-5653; Fax: (847) 491-7713.; (T.L.P.) poulos@uci.edu; Phone: (949) 824-7020; Fax: (949) 824-3280.

Supporting Information

Details regarding the chemical synthesis of **20**, the chemical structure of molecules studied, a table of crystallographic statistics for all ligands reported in this study, and an illustrative description of **23** additional bsNOS–inhibitor complexes. The Supporting Information is available free of charge on the ACS Publications website at DOI: 10.1021/acs.biochem.5b00431.

Accession Codes

Coordinates and structure factors have been deposited in the Protein Data Base under accession nos. 4UG5, 4UG6, 4UG7, 4UG8, 4UG9, 4UGA, 4UGB, 4UGC, 4UGD, 4UGE, 4UGF, 4UGG, 4UGH, 4UGI, 4UGJ, 4UGK, 4UGL, 4UGM, 4UGN, 4UGO, 4UGP, 4UGQ, 4UGR, 4UGS, 4UGT, 4UGU, 4UGV, 4UGW, 4UGX, and 4UGY.

Notes

The authors declare no competing financial interest.

inhibitors reported here provide a revised structural framework for the development of new antimicrobials that target bacterial NOS. In addition, mutagenesis studies reveal several key residues that unlock access to bacterial NOS surfaces that could provide the selectivity required to develop potent bacterial NOS inhibitors.

Graphical abstract

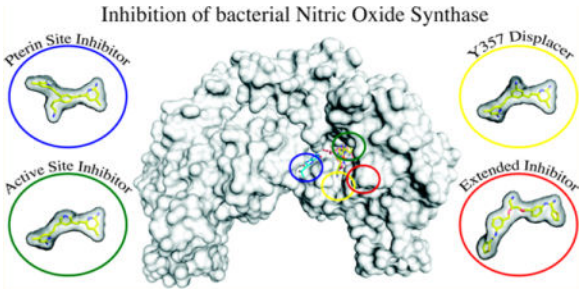

Nitric oxide (NO) is a critical signaling molecule produced by nitric oxide synthase (NOS). Dysregulation in NO signaling leads to a variety of pathophysiological conditions in mammals. These conditions include neurodegeneration,[1] septic shock,[2] and tumor development.[3] Our group and others have focused on the development of competitive active site NOS inhibitors that both mitigate production of NO and demonstrate isoform selectivity for one of the three mammalian NOS isoforms: neuronal NOS (nNOS), inducible NOS (iNOS), or endothelial NOS (eNOS). In fact, several nNOS inhibitors have now been demonstrated to function as potential drugs for melanoma[4] and neurodegenerative diseases.[5] As a direct result of this previous work, a large and chemically diverse library of NOS inhibitors with varying potencies and specificities has been developed.[6,7]

With the advent of bacterial genome sequencing, bacterial NOS (bNOS) homologues have also been identified in several Gram-positive bacteria. Current evidence indicates the role of bNOS to be varied among organisms ranging from nitrosylation of macromolecules[8,9] to functioning as a commensal molecule[10] to enhancing pathogen virulence.[11] In pathogenic organisms *Bacillus anthracis* and *Staphylococcus aureus*, gene deletion experiments first indicated that bNOS plays an important role in ameliorating oxidative and antibiotic stress.[12–14] Recently, we also demonstrated that NOS inhibitors, originally designed to target nNOS, also function as antimicrobials in *Bacillus subtilis*,[15,16] a nonpathogenic model organism for *B. anthracis*. These studies were the first to demonstrate the ability of NOS inhibitors to improve the efficacy of antimicrobials. Therefore, bNOS may serve as a useful therapeutic target for costly pathogens like *B. anthracis* and methicillin-resistant *S. aureus* that also utilize NO to mitigate oxidative and antibiotic stresses.

Unfortunately, application of a generic NOS inhibitor for treatment of a Gram-positive infection would likely do more harm than good in humans. To exploit bNOS as a therapeutic target, specificity must be improved. Specificity against eNOS and iNOS is especially important, considering the essential role eNOS plays in maintaining blood-pressure homeostasis[17] and the important role iNOS plays in pathogen clearance.[18] Limiting eNOS specificity is further complicated by the fact that both bNOS and eNOS share an Asn residue

at the carboxylate binding site of substrate L-Arg. The differences in electrostatics contributed by the Asn (Asp residue in nNOS and iNOS) have been useful for designing selective nNOS inhibitors.[7,19] Recently, we also reported on several inhibitors with antimicrobial activity that targeted both the active and pterin binding sites of bNOS.[16] Since a cosubstrate pterin group is required for NOS catalysis,[20] inhibitors that bind to both the active and pterin sites are an attractive option for limiting NO production. Further development of inhibitors that block pterin binding represents one potential strategy for improving bNOS specificity since pterin binding affinity is drastically different between bNOS and mNOS: micromolar affinity[21] for bNOS vs nanomolar affinity for mNOS.[22]

To advance our understanding of the structural underpinnings that govern bNOS selectivity, we report here over 28 different bNOS–inhibitor crystal structures. Additional characterization through mutagenesis and binding studies has led to the recognition of new hot spots that could prove to be useful toward future bNOS inhibitor design efforts. In particular, we identify a conserved Tyr near the active site that adopts an alternative rotameric position to make available a binding surface unique to bacterial NOS.

EXPERIMENTAL PROCEDURES

Site-Directed Mutagenesis

Previously, we found that the *B. subtilis* NOS (bsNOS) expression plasmid containing sERP[23] mutations E25A/E26A/E316A facilitated protein crystal growth for X-ray studies.[15] Hence, bsNOS mutation Y357F was introduced by site-directed mutagenesis to the E25A/E26A/E316A bsNOS expression plasmid using PFUturbo (Agilent) as the DNA polymerase.

Expression and Purification

Overexpression and isolation of bsNOS from *Escherichia coli* was performed as previously described.[24] To prepare protein for X-ray crystal structure studies, the N-terminal 6×-His tag was removed by incubation with thrombin overnight at 4°C. Cleaved protein was then isolated by an additional passage through a Ni-NTA column. As a final purification step, the bsNOS protein was run over an S75 column containing 25 mM Bis-Tris methane, 75 mM NaCl, 2% (v/v) glycerol, 0.5% (w/v) PEG 3350, and 1 mM DTT at pH 7.4 as the running buffer.

Inhibitor Binding Analysis

The previously reported imidazole spin shift assay was used to evaluate binding of inhibitors to bsNOS.[25,26] In short, the difference between the imidazole-bound low-spin peak at 430 nm and the inhibitor-bound high-spin peak at 395 nm was measured as a function of inhibitor concentration. The data were then fit to a one-site ligand-binding curve using SigmaPlot, version 10.0 (Systat Software, Inc., www.sigmaplot.com). The calculated KS,app was then used to calculate K_S based on the K_D of imidazole at 384 μM,[27] as previously discussed.[26]

X-ray Structure Determination

Crystals of WT bsNOS containing the sERP mutations were prepared as previously described.[15] Mutant containing bsNOS crystals were initially grown from crystal seeds of the WT bsNOS crystals. The resulting crystals were then used to prepare additional mutant crystal seed stocks. The mutant crystal seed stocks were used to grow crystals for X-ray data collection. Crystals were cryoprotected in the well solution[15] supplemented with 30% (v/v) glycerol and 2 mM H_4B. After the cryoprotection step, crystals were soaked in the presence of 5–10 mM inhibitor for 1–3 h prior to flash freezing. X-ray data sets were collected on individual orthorhombic crystals at both the Stanford Synchrotron Radiation Light source (Palo Alto, CA) and the Advanced Light source (Berkeley, CA). Raw data frames were indexed with either XDS[28] or iMOSFLM.[29] In order to scale, and in several cases merge, a high- and low-resolution data set, the program AIMLESS[30] was used. In several cases, data sets suffered from high anisotropy and were further truncated/scaled using the Diffraction Anisotropy Server.[23] Data sets were initially refined using Refmac[31] and the starting model PDB 4D3T. Additional rounds of refinement and TLS refinement were done using PHENIX.[32] The molecular graphics program COOT[33] was used for modeling. Figures were generated using PyMOL.[34]

RESULTS

Sequence- and Structure-Based Differences among NOS Isoforms

The design of selective bNOS inhibitors is difficult owing to the high sequence similarity among human NOS isoforms. In fact, saNOS shares in the range of 41–43% sequence identify with the human mNOS oxygenase domains; sequence identity was evaluated with Clustal W.[52] At the active site alone, saNOS and nNOS share 8 out 10 residues within 5 Å of the native substrate L-Arg. The residue differences correspond to an Asn residue present at the L-Arg carboxylate binding site and an Ile residue that is positioned above the distal plane of the heme. Since eNOS also contributes an Asn residue at the L-Arg carboxylate binding site, inhibitors that target this electrostatic difference are not expected to be very selective. The second residue difference contributed by an Ile in bNOS is a Val in mNOS isoforms. Interestingly, the slightly bulkier Ile functions to lower NO release rates in bNOS.[27]

Figure 1 presents structure-based sequence alignments between *B. subtilis* NOS (bsNOS) and mammalian NOS isoforms. Although the important pathogens *S. aureus* and *B. anthracis* are the therapeutic targets, we used *B. subtilis* NOS for our crystallographic studies because bsNOS crystals diffract to a higher resolution. Moreover, bsNOS and saNOS sequences are 96% consistent and 53% identical based on a T-Coffee[35] and Clustal W[52] sequence alignment, respectively; hence, bsNOS is a suitable model to study saNOS. The largest difference between the bacterial and mammalian NOS isoforms is the absence of an N-terminal Zn^{2+} binding motif in bNOS. The N-terminal Zn^{2+} binding motif is critical for dimerization in mammalian NOS isoforms and is absent in bNOS. Consequently, there is a large cleft at the dimerization interface that is a potential target for inhibitor design. This open pocket encompasses the pterin cofactor binding site. Recently, several inhibitors were demonstrated to have a decreased selectivity for mNOS isoforms owing to the presence of a bulky pharmacophore that bound to the pterin site.[16] As shown in Figure 1, residues adjacent

to the pterin site, like R344 and S345, are unique to the bNOS, which indicates inhibitor design could be further improved by exploiting these differences.

There are additional residue differences (Figure 1) among NOS isoforms near heme propionate group A. Neither H128 nor K360 in *B. subtilis* is conserved in mNOS isoforms. Interestingly, H128 was recently implicated, through a molecular dynamics simulation, to limit the conformational dynamics of one specific inhibitor due to sterics.[16] Additional sequence differences are observed near bsNOS Y357, including N354 and F356. Adjacent to Y357 is also the N-terminal Zn^{2+} binding motif. Hence, inhibitors that bind to this region and do not bind to the N-terminal Zn^{2+} binding motif may also serve as excellent lead compounds for future structure-based inhibitor design.

Inhibitor Binding

Imidazole displacement has proven to be an excellent assay for quantifying the spectral binding affinity (K_S) of NOS inhibitors on the basis of the transition from an imidazole-bound low-spin state to an inhibitor-bound high-spin state. As a first step toward characterization of inhibitor binding, we analyzed **28** NOS inhibitors (Supporting Information, Figure S1) that have previously been characterized to bind to mNOS isoforms. Consistent with previous results,[15,16] all inhibitors evaluated bind to bsNOS in the low micromolar range (Table 1).

Pterin Site Binding

NOS inhibitors that target the pterin site have previously been demonstrated to have antimicrobial properties against *B. subtilis*.[15,16] Crystal structure analyses revealed two additional compounds, **5** and **15**, that interact with the pterin site. In the case of **5**, one of the aminopyridine groups displaces the pterin molecule in order to H-bond with heme propionate D (Figure 2). This binding motif has previously been observed in bNOS with inhibitors containing two aminopyridine groups.[15,16] Identification of inhibitors that bind to the pterin site is interesting because the open cavity adjacent to the pterin binding site is unique to bacterial NOS. In comparison to the binding mode of inhibitor **5** in nNOS, the binding mode of inhibitor **5** in bsNOS is very different (Figure 2C). In the case of nNOS–**5**, the inhibitor interacts with heme propionate A by inducing an alternative conformation in Y706. In several cases, potent nNOS inhibitors have been identified to bind heme propionate A by inducing an alternative conformation in a nearby Tyr.[36] Specifically, the unique binding mode of **5** to nNOS results in a K_i of 0.54 μM.[37] For aminopyridine-based inhibitors, the alternative rotameric position of Tyr results in a tight bifurcated H-bond between the heme propionate and inhibitor. The alternative rotameric position of Tyr is further stabilized by a π–π stacking interaction between the Tyr residue and the aminopyridine-based inhibitors. In nNOS, **5** is likely unable to H-bond with heme propionate D because the binding affinity of H_4B is very tight.[22] Since binding of H_4B to bNOS is weak, **5** can more easily outcompete binding of H_4B.

In the case of **15**, inhibitor binding to bsNOS distorts the pterin binding site by inducing an alternative rotameric position in W329 (Figure 3A). Crystallographic refinement shows residual electron density consistent with an imidazole molecule forming a stacking

interaction with W329. Direct comparison of the binding modes of **15** to bsNOS and nNOS indicates that they are nearly identical (Figure 3A,B). Previous structure–activity analyses have indicated the potency of **15** to vary between nNOS and eNOS, as indicated by K_i values of 0.54 and 12.1 μM,[37] respectively. In both bNOS and nNOS, heme propionate D is in an atypical conformation, with the carboxyl group pointing perpendicular to the plane of the heme. This atypical conformation of heme propionate D induced by **15** binding is likely the cause of the alternative rotameric position of W329.

Tyrosine Flipping Opens a Channel for bNOS Inhibitor Binding

A conserved tyrosine residue in all NOS isoforms H-bonds with heme propionate A This tyrosine has previously been observed to occupy alternative rotameric positions in nNOS to accommodate inhibitors.[36] In several cases, including nNOS–**5** (Figure 2C), inhibitor potency and selectivity are enhanced by the propensity of nNOS Y706 to occupy alternative conformations as a result of the formation of two H-bonds with the heme propionate group.[36] This Tyr is conserved in bsNOS and also adopts alternative conformations in the presence of specific inhibitors. For example, in both bsNOS and nNOS, **3** binds to heme propionate A through a bifurcated H-bond and a π–π stacking interaction between the conserved Tyr and aminopyridine group (Figure 4). This alternative rotameric position at the conserved Tyr results in a K_S of 18.3 ± 2.1 μM for bsNOS (Table 1) and a K_i of 0.056 μM for nNOS. Analogous binding interactions that result in a flipped Y357 in bsNOS are also observed for **1**, **2**, **11**, and **12** (Supporting Information, Figure S2). Moreover, these binding interactions lead to formation of a noncanonical surface that is unique to bNOS, labeled as the open binding surface in Figure 4. This surface is unique to bNOS because of both the drastic differences in surface residues at this site (Figure 1) and the absent Zn^{2+} binding motif (Figure 4).

To better understand the role of Tyr flipping and the H-bond shared between the NOS derived Tyr and the heme propionate group, we introduced the Y357F mutation to bsNOS. Crystal structure analysis of Y357F with L-Arg, a ligand that does not induce Tyr flipping, revealed the rotameric position of Y357F to be nearly identical to that of native Y357 (Figure 5). These data indicate that, aside from the H-bond between Y357 and the heme propionate, there is an energetic barrier between alternative conformations of Y357. Consequently, the “flipped” rotameric position of Y357 can be induced only upon binding of specific ligands. This flipping requires an enthalpically favorable H-bond between the inhibitor and heme propionate groups to overcome the energetic barrier of an alternative rotameric conformation. These thermodynamic considerations are observed with the binding of inhibitor **4** (Figure 6). **4** is an inhibitor that induces a flipped-out conformation in nNOS but not in bsNOS (Figure 6A,B). However, the flipped conformation can be rescued in bsNOS by the introduction of Y357F (Figure 6C). On the basis of the crystal structures, it is clear that from the orientation of **4** that binding is controlled by H-bonds. More specifically the binding of **4** to bsNOS is stabilized by a 3.2 Å H-bond between the pyrrolidine ring and the carbonyl group of H_4B. However, the distance between the H_4B carbonyl group and the pyrrolidine amine is extended to 3.7 Å, as observed in the crystal structure of Y357F bsNOS–**4**, to accommodate the two new H-bonds formed between **4** and heme propionate A (Figure 6C).

Thiophenecarboximidamide Inhibitor Binding

Considerations for improving NOS inhibitor bioavailability have also led to the generation of thiophenecarboximidamide-based NOS inhibitors.[38] These inhibitors preserve a bifurcated H-bond with the active site Glu (Figure 7 and Supporting Information Figure S3). Interestingly, in bNOS, the conjugated ring system of this class of inhibitors forms a hydrophobic interaction with Ile-218. Hence, molecules that utilize this scaffold may lead to improved binding to bNOS because the bNOS active site is slightly more hydrophobic than the mNOS active sites as a result of the Ile/Val difference (Figure 1) even though the binding mode does not change in the I218V mutant bsNOS.[16]

The binding modes of several thiophenecarboximidamide-based inhibitors were found to be unique to bsNOS. Because of the extended length of **23**, **24**, **25**, and **28**, the inhibitors were able to wrap around the active site (Figure 7 and Supporting Information Figure S4). This allows the molecules to access a surface on bsNOS that is not accessible to mNOS isoforms. Specifically, comparison of the binding modes for **24** in bsNOS and nNOS reveals that one of the two thiophenecarboximidamide groups binds very differently between the NOS isoforms. For nNOS, one of the thiophenecarboximidamide groups is unable to extend outside of the active site because the N-terminal Zn^{2+} binding motif sterically restricts the binding of **24** to the active site. Residues that sterically limit the binding of **24** include L337 and M336 (Figure 7B). In sharp contrast, **24** binds to bsNOS by extending outside the active site to interact with a surface adjacent to Y357 (Figure 7A). This suggests that addition of a bulky pharmacophore to a NOS inhibitor may also prove to be a useful solution for improving specificity toward bNOS, as bulky pharmacophores would likely be unable to interact with the mNOS active sites because of the steric crowding presented by the N-terminal Zn^{2+} binding motif.

DISCUSSION

The NOS inhibitor design effort has largely been aided by the structural characterization of NOS–inhibitor interactions.[7] These studies have been indispensible to providing a molecular understanding of residues that govern isoform selectivity and useful pharmacophores. Since the previous application of mNOS inhibitors to a bacterial system has proven them to function as a potential antimicrobial target,[15,16] a renewed understanding of NOS isoform selectivity is needed to exploit the bNOS system. To further our understanding of bNOS inhibitor interactions, we solved numerous bsNOS–inhibitor crystal structures. From these studies, we have identified four design features that could potentially result in more selective bNOS inhibitors.

First, the bNOS active site has and Ile, whereas mNOS has a Val. The slight difference in hydrophobicity and sterics between the NOS active site has previously been identified to influence the kinetics of NO dissociation.[27] From our crystal structure analysis, the bsNOS I218 may also facilitate binding of NOS inhibitors to the bNOS active site. Specifically, these inhibitors include the thiophenecarboximidamide-based inhibitors reported in this study. Binding of inhibitors **19**–**28** results in a hydrophobic contact between the I218 side chain and the benzyl moiety of the inhibitor.

Second, Y357 can adopt an alternative rotameric position upon inhibitor binding. The alternative rotameric position of Y357 allows inhibitors to interact with heme propionate A. Similar studies with eNOS and nNOS have shown that the corresponding Tyr is more easily displaced in nNOS than in eNOS.[36] Since this Tyr is also displaced in bNOS, inhibitors that favor movement of the Tyr should be more selective for bNOS over eNOS but not for nNOS. However, since inhibition of nNOS requires penetration of the blood–brain barrier, which has proven to be a limitation for selective targeting of nNOS, selectivity over nNOS is not a major concern.

Third, inhibitors that bind to the pterin site should also be selective for bNOS. Pterins bind much more weakly to bNOS than to any of the mNOS isoforms. This is because bNOS lacks the mNOS Zn^{2+} binding motif that is present at the dimer interface. As a result, the pterin site in bNOS is more solvent-exposed and less defined than the mNOS pterin site. In other words, this structural difference both lowers affinity for pterins to bNOS and provides a much larger pocket for which a bulky pharmacophore could bind. Targeting of the bNOS pterin site might prove to be useful as a bulky pharmacophore could favor binding to bNOS over mNOS. From our initial studies,[15,16] we identified several inhibitors with two aminopyridine groups that work to displace the pterin in bsNOS and H-bond to heme propionate A In contrast, these same inhibitors were observed to displace a conserved Tyr to H-bond with heme propionate D in nNOS. This provides an important lesson for future inhibitor design. A pharmacophore that is bulkier than an aminopyridine and capable of H-bonding to heme propionate D should both displace the pterin in bsNOS and, based on sterics, be too big to interact with either of the mNOS heme propionate groups.

Fourth, the differences in the binding of **24** to bsNOS and nNOS points to another unique pocket in bNOS that can be exploited for selective inhibitor design. The tail end of the thiophenecarboximidamide extends in the opposite direction compared to that in nNOS. This binding mode is not observed in nNOS due to steric clashes at the dimer interface afforded by the presence of the Zn^{2+} binding motif. In summary, the overall general design principle is to develop inhibitors that interact with the active site Glu as in all NOS isoforms but that take advantage residue differences like Ile-218 and the additional nonpolar interactions unique to the bNOS active site and pterin binding site to improve bNOS inhibitor binding. The tail end of the inhibitor extending out of the active site should be bulky to favor binding the more open bNOS dimer interface but retain the ability to H-bond with one of the heme propionates by either displacing the pterin or forcing Y357 to adopt the alternative rotameric orientation.

Supplementary Material

Refer to Web version on PubMed Central for supplementary material.

Acknowledgments

A special thanks is extended to Dr. Huiying Li for his many excellent discussions regarding data processing and inhibitor binding. We also thank the beamline staff at the Advanced Light Source and the Stanford Synchrotron Radiation Light source (Palo Alto, CA) for help with remote data collection.

Funding

This work was supported by NIH grant nos. GM57353 (to T.L.P.) and GM49725 (to R.B.S.).

ABBREVIATIONS

NOS	nitric oxide synthase
NO	nitric oxide
nNOS	neuronal nitric oxide synthase
eNOS	endothelial nitric oxide synthase
iNOS	inducible nitric oxide synthase
bNOS	bacterial nitric oxide synthase
bsNOS	*Bacillus subtilis* nitric oxide synthase
saNOS	*Staphylococcus aureus* nitric oxide synthase

References

1. Hunot S, Boissiere F, Faucheux B, Brugg B, Mouatt-Prigent A, Agid Y, Hirsch EC. Nitric oxide synthase and neuronal vulnerability in Parkinson's disease. Neuroscience. 1996; 72:355–363. [PubMed: 8737406]
2. Thiemermann C. Nitric oxide and septic shock. Gen Pharmacol. 1997; 29:159–166. [PubMed: 9251894]
3. Singh S, Gupta AK. Nitric oxide: role in tumour biology and iNOS/NO-based anticancer therapies. Cancer Chemother Pharmacol. 2011; 67:1211–1224. [PubMed: 21544630]
4. Yang Z, Misner B, Ji H, Poulos TL, Silverman RB, Meyskens FL, Yang S. Targeting nitric oxide signaling with nNOS inhibitors as a novel strategy for the therapy and prevention of human melanoma. Antioxid Redox Signaling. 2013; 19:433–447.
5. Ji H, Tan S, Igarashi J, Li H, Derrick M, Martasek P, Roman LJ, Vasquez-Vivar J, Poulos TL, Silverman RB. Selective neuronal nitric oxide synthase inhibitors and the prevention of cerebral palsy. Ann Neurol. 2009; 65:209–217. [PubMed: 19235180]
6. Silverman RB. Design of selective neuronal nitric oxide synthase inhibitors for the prevention and treatment of neurodegenerative diseases. Acc Chem Res. 2009; 42:439–451. [PubMed: 19154146]
7. Poulos TL, Li H. Structural basis for isoform-selective inhibition in nitric oxide synthase. Acc Chem Res. 2013; 46:390–398. [PubMed: 23030042]
8. Johnson EG, Sparks JP, Dzikovski B, Crane BR, Gibson DM, Loria R. Plant-pathogenic Streptomyces species produce nitric oxide synthase-derived nitric oxide in response to host signals. Chem Biol. 2008; 15:43–50. [PubMed: 18215772]
9. Buddha MR, Keery KM, Crane BR. An unusual tryptophanyl tRNA synthetase interacts with nitric oxide synthase in *Deinococcus radiodurans*. Proc Natl Acad Sci USA. 2004; 101:15881–15886. [PubMed: 15520379]
10. Gusarov I, Gautier L, Smolentseva O, Shamovsky I, Eremina S, Mironov A, Nudler E. Bacterial nitric oxide extends the lifespan of *C. elegans*. Cell. 2013; 152:818–830. [PubMed: 23415229]
11. van Sorge NM, Beasley FC, Gusarov I, Gonzalez DJ, von Kockritz-Blickwede M, Anik S, Borkowski AW, Dorrestein PC, Nudler E, Nizet V. Methicillin-resistant *Staphylococcus aureus* bacterial nitric-oxide synthase affects antibiotic sensitivity and skin abscess development. J Biol Chem. 2013; 288:6417–6426. [PubMed: 23322784]
12. Gusarov I, Nudler E. NO-mediated cytoprotection: instant adaptation to oxidative stress in bacteria. Proc Natl Acad Sci USA. 2005; 102:13855–13860. [PubMed: 16172391]
13. Gusarov I, Shatalin K, Starodubtseva M, Nudler E. Endogenous nitric oxide protects bacteria against a wide spectrum of antibiotics. Science. 2009; 325:1380–1384. [PubMed: 19745150]

14. Shatalin K, Gusarov I, Avetissova E, Shatalina Y, McQuade LE, Lippard SJ, Nudler E. *Bacillus anthracis*-derived nitric oxide is essential for pathogen virulence and survival in macrophages. Proc Natl Acad Sci USA. 2008; 105:1009–1013. [PubMed: 18215992]
15. Holden JK, Li H, Jing Q, Kang S, Richo J, Silverman RB, Poulos TL. Structural and biological studies on bacterial nitric oxide synthase inhibitors. Proc Natl Acad Sci USA. 2013; 110:18127–18131. [PubMed: 24145412]
16. Holden JK, Kang S, Hollingsworth SA, Li H, Lim N, Chen S, Huang H, Xue F, Tang W, Silverman RB, Poulos TL. Structure-based design of bacterial nitric oxide synthase inhibitors. J Med Chem. 2015; 58:994–1004. [PubMed: 25522110]
17. Forstermann U, Sessa WC. Nitric oxide synthases: regulation and function. Eur Heart J. 2012; 33:829–837. [PubMed: 21890489]
18. Bogdan C. Nitric oxide and the immune response. Nat Immunol. 2001; 2:907–916. [PubMed: 11577346]
19. Flinspach ML, Li H, Jamal J, Yang W, Huang H, Hah JM, Gomez-Vidal JA, Litzinger EA, Silverman RB, Poulos TL. Structural basis for dipeptide amide isoform-selective inhibition of neuronal nitric oxide synthase. Nat Struct Mol Biol. 2004; 11:54–59. [PubMed: 14718923]
20. Adak S, Aulak KS, Stuehr DJ. Direct evidence for nitric oxide production by a nitric-oxide synthase-like protein from *Bacillus subtilis*. J Biol Chem. 2002; 277:16167–16171. [PubMed: 11856757]
21. Crane BR, Sudhamsu J, Patel BA. Bacterial nitric oxide synthases. Annu Rev Biochem. 2010; 79:445–470. [PubMed: 20370423]
22. Tejero J, Stuehr D. Tetrahydrobiopterin in nitric oxide synthase. IUBMB Life. 2013; 65:358–365. [PubMed: 23441062]
23. Strong M, Sawaya MR, Wang S, Phillips M, Cascio D, Eisenberg D. Toward the structural genomics of complexes: crystal structure of a PE/PPE protein complex from *Mycobacterium tuberculosis*. Proc Natl Acad Sci USA. 2006; 103:8060–8065. [PubMed: 16690741]
24. Pant K, Bilwes AM, Adak S, Stuehr DJ, Crane BR. Structure of a nitric oxide synthase heme protein from *Bacillus subtilis*. Biochemistry. 2002; 41:11071–11079. [PubMed: 12220171]
25. Holden JK, Lim N, Poulos TL. Identification of redox partners and development of a novel chimeric bacterial nitric oxide synthase for structure activity analyses. J Biol Chem. 2014; 289:29437–29445. [PubMed: 25194416]
26. Roman LJ, Sheta EA, Martasek P, Gross SS, Liu Q, Masters BS. High-level expression of functional rat neuronal nitric oxide synthase in *Escherichia coli*. Proc Natl Acad Sci USA. 1995; 92:8428–8432. [PubMed: 7545302]
27. Wang ZQ, Wei CC, Sharma M, Pant K, Crane BR, Stuehr DJ. A conserved Val to Ile switch near the heme pocket of animal and bacterial nitric-oxide synthases helps determine their distinct catalytic profiles. J Biol Chem. 2004; 279:19018–19025. [PubMed: 14976216]
28. Kabsch W. Xds. Acta Crystallogr, Sect D: Biol Crystallogr. 2010; 66:125–132. [PubMed: 20124692]
29. Battye TG, Kontogiannis L, Johnson O, Powell HR, Leslie AG. iMOSFLM: a new graphical interface for diffraction-image processing with MOSFLM. Acta Crystallogr, Sect D: Biol Crystallogr. 2011; 67:271–281. [PubMed: 21460445]
30. Collaborative Computational Project Number 4. The CCP4 suite: programs for protein crystallography. Acta Crystallogr, Sect D: Biol Crystallogr. 1994; 50:760–763. [PubMed: 15299374]
31. Murshudov GN, Vagin AA, Dodson EJ. Refinement of macromolecular structures by the maximum-likelihood method. Acta Crystallogr, Sect D: Biol Crystallogr. 1997; 53:240–255. [PubMed: 15299926]
32. Adams PD, Afonine PV, Bunkoczi G, Chen VB, Davis IW, Echols N, Headd JJ, Hung LW, Kapral GJ, Grosse-Kunstleve RW, McCoy AJ, Moriarty NW, Oeffner R, Read RJ, Richardson DC, Richardson JS, Terwilliger TC, Zwart PH. PHENIX: a comprehensive Python-based system for macromolecular structure solution. Acta Crystallogr, Sect D: Biol Crystallogr. 2010; 66:213–221. [PubMed: 20124702]

33. Emsley P, Lohkamp B, Scott WG, Cowtan K. Features and development of Coot. Acta Crystallogr, Sect D: Biol Crystallogr. 2010; 66:486–501. [PubMed: 20383002]
34. The PyMOL Molecular Graphics System, version 1.3r1. Schrödinger, LLC; New York: 2010.
35. Notredame C, Higgins DG, Heringa J. T-Coffee: A novel method for fast and accurate multiple sequence alignment. J Mol Biol. 2000; 302:205–217. [PubMed: 10964570]
36. Li H, Jamal J, Delker S, Plaza C, Ji H, Jing Q, Huang H, Kang S, Silverman RB, Poulos TL. The mobility of a conserved tyrosine residue controls isoform-dependent enzymeinhibitor interactions in nitric oxide synthases. Biochemistry. 2014; 53:5272–5279. [PubMed: 25089924]
37. Huang H, Li H, Martasek P, Roman LJ, Poulos TL, Silverman RB. Structure-guided design of selective inhibitors of neuronal nitric oxide synthase. J Med Chem. 2013; 56:3024–3032. [PubMed: 23451760]
38. Huang H, Silverman RB. Recent advances toward improving the bioavailability of neuronal nitric oxide synthase inhibitors. Curr Top Med Chem. 2013; 13:803–812. [PubMed: 23578024]
39. Delker SL, Xue F, Li H, Jamal J, Silverman RB, Poulos TL. Role of zinc in isoform-selective inhibitor binding to neuronal nitric oxide synthase. Biochemistry. 2010; 49:10803–10810. [PubMed: 21138269]
40. Kang S, Li H, Tang W, Martasek P, Roman LJ, Poulos TL, Silverman RB. 2-Aminopyridines with a truncated side chain to improve human neuronal nitric oxide synthase potency and selectivity. J Med Chem. 2015
41. Holden JK, Kang S, Beasley FC, Cinelli MA, Li H, Roy SG, Dejam D, Edinger AL, Nizet V, Silverman RB, Poulos TL. Nitric oxide synthase as a target for methicillin-resistant. Staphylococcus aureus Chem Biol. 2015
42. Huang H, Ji H, Li H, Jing Q, Labby KJ, Martasek P, Roman LJ, Poulos TL, Silverman RB. Selective monocationic inhibitors of neuronal nitric oxide synthase. Binding mode insights from molecular dynamics simulations. J Am Chem Soc. 2012; 134:11559–11572. [PubMed: 22731813]
43. Huang H, Li H, Yang S, Chreifi G, Martasek P, Roman LJ, Meyskens FL, Poulos TL, Silverman RB. Potent and selective double-headed thiophene-2-carboximidamide inhibitors of neuronal nitric oxide synthase for the treatment of melanoma. J Med Chem. 2014; 57:686–700. [PubMed: 24447275]
44. Jing Q, Li H, Fang J, Roman LJ, Martasek P, Poulos TL, Silverman RB. In search of potent and selective inhibitors of neuronal nitric oxide synthase with more simple structures. Bioorg Med Chem. 2013; 21:5323–5331. [PubMed: 23867386]
45. Jing Q, Li H, Chreifi G, Roman LJ, Martasek P, Poulos TL, Silverman RB. Chiral linkers to improve selectivity of double-headed neuronal nitric oxide synthase inhibitors. Bioorg Med Chem Lett. 2013; 23:5674–5679. [PubMed: 23993333]
46. Jing Q, Li H, Roman LJ, Martasek P, Poulos TL, Silverman RB. Combination of chiral linkers with thiophenecarboximidamide heads to improve the selectivity of inhibitors of neuronal nitric oxide synthase. Bioorg Med Chem Lett. 2014; 24:4504–4510. [PubMed: 25149509]
47. Jing Q, Li H, Roman LJ, Martasek P, Poulos TL, Silverman RB. An accessible chiral linker to enhance potency and selectivity of neuronal nitric oxide synthase inhibitors. ACS Med Chem Lett. 2014; 5:56–60. [PubMed: 24660051]
48. Kang S, Tang W, Li H, Chreifi G, Martasek P, Roman LJ, Poulos TL, Silverman RB. Nitric oxide synthase inhibitors that interact with both heme propionate and tetrahydrobiopterin show high isoform selectivity. J Med Chem. 2014; 57:4382–4396. [PubMed: 24758147]
49. Silverman, RB.; Huang, H.; Jing, Q. Thiophene-2-carboximidamide Based Selective Neuronal Nitric Oxide Inhibitors. US Patent. 8,735,606. 2014.
50. Celniker G, Nimrod G, Ashkenazy H, Glaser F, Martz E, Mayrose I, Pupko T, Ben-Tal N. ConSurf: using evolutionary data to raise testable hypotheses about protein function. Isr J Chem. 2013; 53:199–206.
51. Pettersen EF, Goddard TD, Huang CC, Couch GS, Greenblatt DM, Meng EC, Ferrin TE. UCSF chimera—a visualization system for exploratory research and analysis. J Comput Chem. 2004; 25:1605–1612. [PubMed: 15264254]

52. Larkin MA, Blackshields G, Brown NP, Chenna R, McGettigan PA, McWilliam H, Valentin F, Wallace IM, Wilm A, Lopez R, Thompson JD, Gibson TJ, Higgins DG. Clustal W and clustal X version 2.0. Bioinformatics. 2007; 23:2947–2948. [PubMed: 17846036]

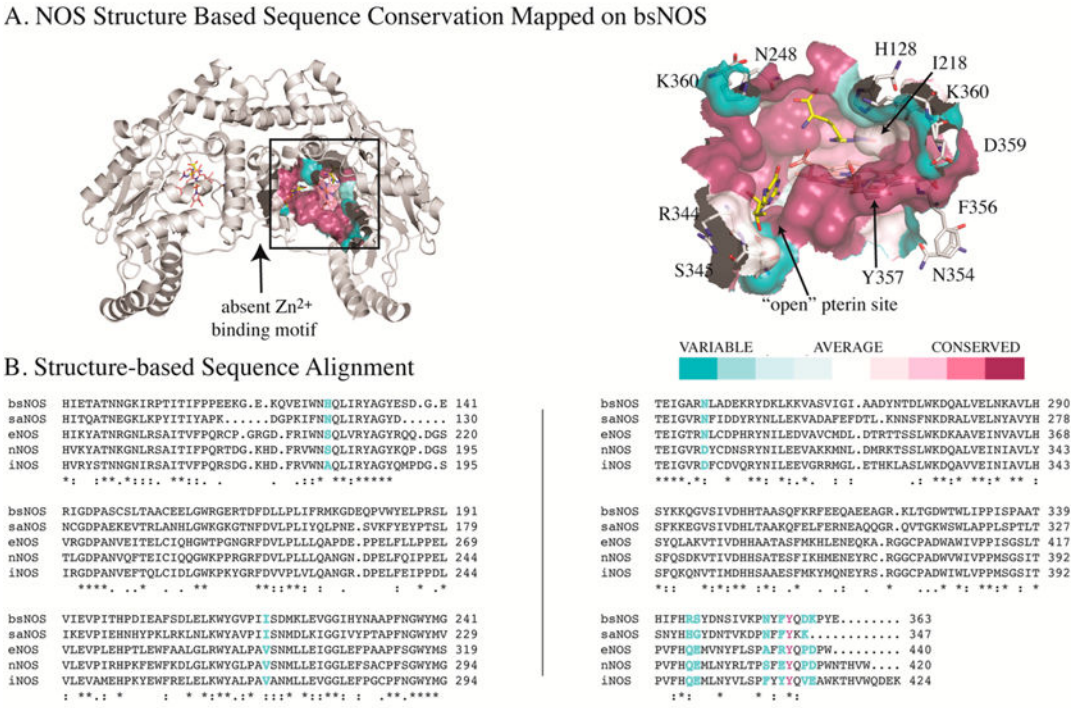

Figure 1.

(A) Crystal structure of bsNOS (PDB 4UQR) shown as a dimer with active site conservation colored using the consurf web server.[50,51] (B) Partial sequence alignment of NOS isoforms based on a structural alignment using Chimera and crystal structures of bsNOS (PDB 4UQR), saNOS (PDB 1MJT), human eNOS (PDB 4D1O), human nNOS (PDB 4D1N), and human iNOS (PDB 3E7G). Residues identified on the bsNOS crystal structure in (A) are also colored in (B).

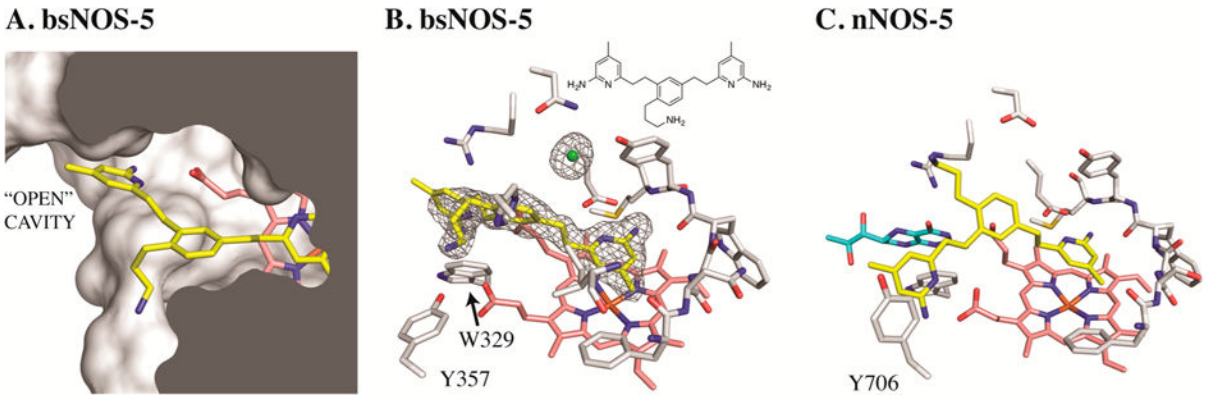

Figure 2.

(A) **5** bound to bsNOS with the aminopyridine group bound to the heme propionate and exposed to a solvent-accessible surface that is unique to bNOS. (B) Stick representation and $2F_o - F_c$ at 1.0σ of **5** bound to bsNOS. (C) Stick representation of nNOS–**5** (PDB 4IMT). In all representations, the heme group is salmon, **5** is yellow, a chlorine ion is green, H_4B is cyan, and the protein residues are white.

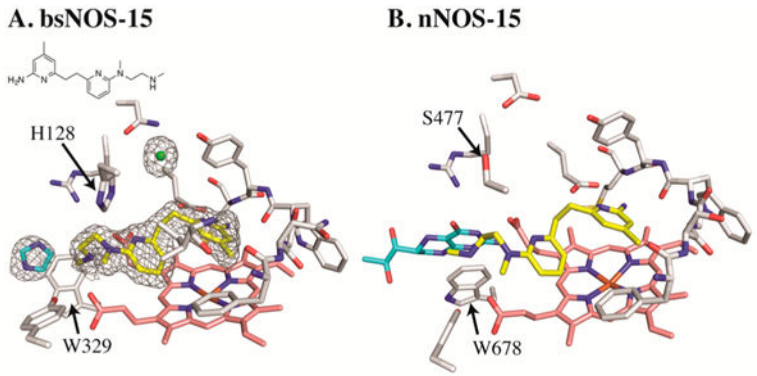

Figure 3.

15 binds in a near identical conformation to both (A) bsNOS and (B) nNOS (PDB 4UH0). In the case of bsNOS–**15**, a torque is applied to W329, and the pterin site is distorted. $2F_o - F_c$ maps for ligands and a chlorine ion are shown at 1.0σ. In both models, the heme group is salmon, **15** is yellow, select active site residues are displayed as white sticks, a chlorine anion is a green, and both imidazole and H_4B are cyan.

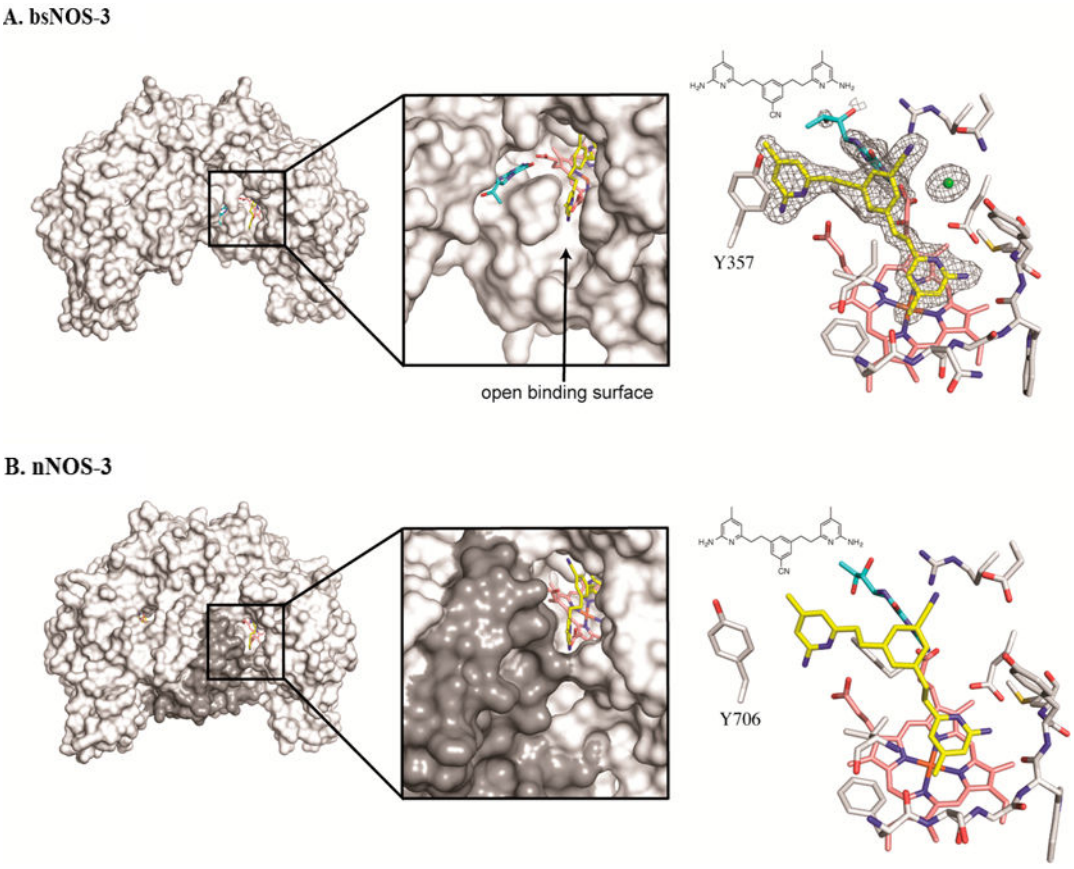

Figure 4.

Inhibitor **3** induces a conformational change in both (A) bsNOS Y357 and (B) nNOS Y706. Rotation of Y357 in bsNOS opens access to a novel binding surface depicted in A. Surface representations of NOS oxygenase domains as dimers are white, with the N-terminal Zn^{2+} motif in gray. Heme groups are salmon, and ligands are yellow. The $2F_o - F_c$ map for bsNOS–**3** is show at 1.0σ. The nNOS–**3** models were generated using PDB 4IMW.

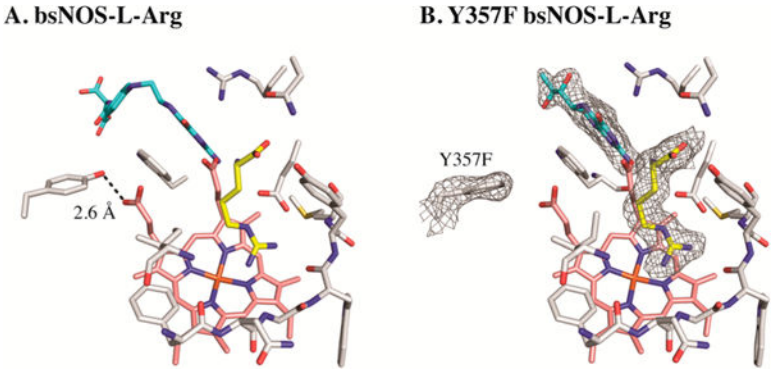

Figure 5.

(A) Active site view of L-Arg and tetrahydrofolate bound to bsNOS (redrawn from PDB 1M7V). (B) Y357F bsNOS with L-Arg and H_4B bound and shown with a $2F_o - F_c$ map contoured at 1.0σ. Protein residues of the NOS active site are white, heme is salmon, the pterin group is cyan, and L-Arg is yellow.

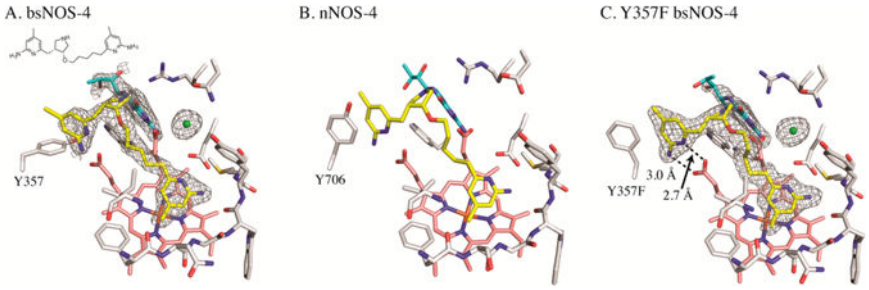

Figure 6.

Inhibitor **4** bound to NOS active site shown as yellow sticks with the heme group in salmon, protein residues in white, and H_4B in cyan. (A) The $2F_o - F_c$ map is contoured at 1.0σ for bsNOS–**4**. (B) **4** binds to nNOS by coordinating to the heme propionate group. (C) 4 binding to bsNOS is able to coordinate to the heme propionate only by introduction of mutation Y357F. The $2F_o - F_c$ map of **4** and H_4B is contoured at 1.0σ.

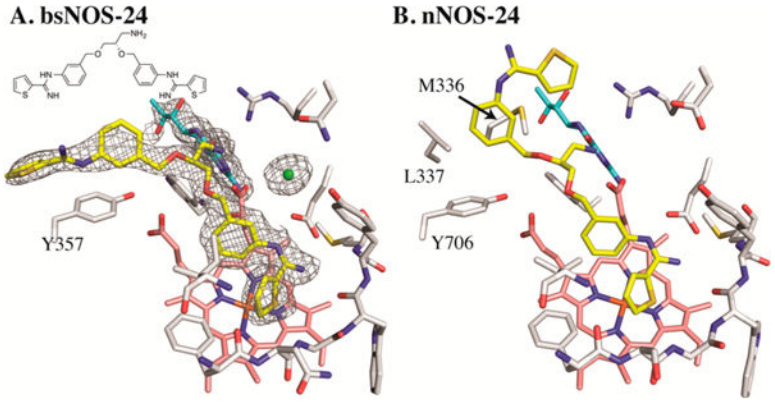

Figure 7.

(A) Binding mode of **24** to bsNOS is extended to accommodate binding on the surface of the protein outside of the active site. The $2F_o - F_c$ map of **24**, H_4B, and the active site chloride anion are contoured at 1.0σ. (B) **24** binding to nNOS results from the partially blocked active site, contributed by residues L337 and M336 (redrawn from PDB 4UPN). The color scheme shown has H_4B in cyan, **24** in yellow, heme in salmon, and protein residues in white.

Table 1

Comparison of Inhibitor Binding to bsNOS[a]

inhibitor	K_S (μM)	synthesis reported	inhibitor	K_S (μM)	synthesis reported
1	5.03 ± 0.04	39	**15**	18.3 ± 2.1	40
2	2.68 ± 0.12	39	**16**	n.d.	40
3	4.47 ± 0.36	37	**17**	22.3 ± 0.8	41
4	0.45 ± 0.05	42	**18**	62.14 ± 3.59	41
5	8.61 ± 0.50	37	**19**	99 ± 20	43
6	61.0 ± 3.5	44	**20**	17.8 ± 2.0	reported here
7	237 ± 24	44	**21**	62.3 ± 7.6	43
8	18.7 ± 7.1	45	**22**	n.d.	43
9	37.9 ± 2.2	45	**23**	169 ± 31	46
10	n.d.	44	**24**	n.d.	46
11	23.3 ± 2.2	47	**25**	11.0 ± 0.8	46
12	25.6 ± 0.7	48	**26**	127 ± 44	43
13	50.46 ± 3.56	40	**27**	72.4 ± 8.9	49
14	57.6 ± 8.7	40	**28**	7.73 ± 0.43	46

[a]Inhibitor binding using the imidazole displacement assay indicates inhibitors studied here bind in the low micromolar range. Spectral binding constants that were not determined are indicated by n.d.